Nuclear Engineering and Technology 55 (2023) 884–894

Contents lists available at ScienceDirect

Nuclear Engineering and Technology

journal homepage: www.elsevier.com/locate/net

Original Article

Assessment of INSPYRE-extended fuel performance codes against the SUPERFACT-1 fast reactor irradiation experiment

L. Luzzi [a,*], T. Barani [a], B. Boer [b], A. Del Nevo [c], M. Lainet [d], S. Lemehov [b], A. Magni [a], V. Marelle [d], B. Michel [d], D. Pizzocri [a], A. Schubert [e], P. Van Uffelen [e], M. Bertolus [d]

[a] Politecnico di Milano, Department of Energy, Nuclear Engineering Division, Via La Masa 34, 20156, Milano, Italy
[b] Belgian Nuclear Research Centre SCK·CEN, Boeretang 200, 2400, Mol, Belgium
[c] ENEA, FSN-ING-SIS, CR Brasimone, 40032, Camugnano (BO), Italy
[d] Commissariat à l'Energie Atomique et aux Energies Alternatives, CEA DEC/SESC, 13108 St. Paul Lez Durance, France
[e] European Commission, Joint Research Centre, Directorate for Nuclear Safety and Security, P.O. Box 2340, 76125, Karlsruhe, Germany

ARTICLE INFO

Article history:
Received 29 July 2022
Received in revised form
18 October 2022
Accepted 27 October 2022
Available online 31 October 2022

Keywords:
MOX fuel
SUPERFACT-1 irradiation experiment
Fuel performance codes
GERMINAL
MACROS
TRANSURANUS
Assessment and benchmark

ABSTRACT

Design and safety assessment of fuel pins for application in innovative Generation IV fast reactors calls for a dedicated nuclear fuel modelling and for the extension of the fuel performance code capabilities to the envisaged materials and irradiation conditions. In the INSPYRE Project, comprehensive and physics-based models for the thermal-mechanical properties of U–Pu mixed-oxide (MOX) fuels and for fission gas behaviour were developed and implemented in the European fuel performance codes GERMINAL, MACROS and TRANSURANUS. As a follow-up to the assessment of the reference code versions ("pre-INSPYRE", NET 53 (2021) 3367–3378), this work presents the integral validation and benchmark of the code versions extended in INSPYRE ("post-INSPYRE") against two pins from the SUPERFACT-1 fast reactor irradiation experiment. The post-INSPYRE simulation results are compared to the available integral and local data from post-irradiation examinations, and benchmarked on the evolution during irradiation of quantities of engineering interest (e.g., fuel central temperature, fission gas release). The comparison with the pre-INSPYRE results is reported to evaluate the impact of the novel models on the predicted pin performance. The outcome represents a step forward towards the description of fuel behaviour in fast reactor irradiation conditions, and allows the identification of the main remaining gaps.

1. Introduction

The strategy for most of the Generation IV reactor concepts foresees the use of mixed-oxide nuclear fuel (MOX), i.e., U–Pu fuel potentially including a minor actinide (Am, Np) content for transmutation and recycling purposes [1,2]. These fuels will be subjected to harsh irradiation conditions in terms of fast neutron flux, fuel temperatures and corrosive liquid-metal cooling environment [3]. The design and safety assessment of fuel pins for application in these fast reactors (FRs) calls for a dedicated nuclear fuel modelling and simulation, allowing for the accurate description of the pin behaviour in the irradiation conditions foreseen. Fuel performance codes (FPCs) have been developed since the 1980's to simulate the evolution of fuel pins under determined irradiation and boundary (coolant) conditions, allowing to collect the indications necessary for the pin design and to evaluate the compliance with proper safety margins (e.g., in terms of fuel melting or cladding plasticity) [4,5].

The objective of the INSPYRE European H2020 Project (Investigations Supporting MOX Fuel Licensing for ESNII Prototype Reactors) [6] is to advance the simulation of MOX fuels by means of:

1) The investigation of properties of these fuels and phenomena occurring under irradiation using a combination of experimental techniques and lower-length scale and thermodynamic calculations.
2) The development of advanced models including the knowledge obtained and their implementation in fuel performance codes, extending the FPC predictive capabilities on fast reactor conditions.

The fuel performance codes considered in the INSPYRE Project

* Corresponding author.
E-mail address: lelio.luzzi@polimi.it (L. Luzzi).

https://doi.org/10.1016/j.net.2022.10.038

are: GERMINAL, developed by CEA, France [7,8]; MACROS, from SCK CEN, Belgium [9]; TRANSURANUS, developed by the JRC-Karlsruhe, Germany [10–12] and used extensively by ENEA and Politecnico di Milano. The assessment of the predictive capabilities of the codes prior to the INSPYRE developments ("pre-INSPYRE" versions) on MOX fuel pins irradiated in FR conditions during the SUPERFACT-1 experiment [13] was already published by the same authors [14].

The codes have been extended during the Project by implementing comprehensive and physics-based models for the thermal-mechanical properties of FR MOX fuels, including their evolution under irradiation (i.e., as a function of burn-up), and for the fission gas behaviour and release, as detailed in [15]. In particular, GERMINAL and TRANSURANUS benefited from the integration of:

- Novel correlations for the thermal conductivity, heat capacity (in GERMINAL) and melting temperature of MOX fuels [16–19].
- Novel correlations for the thermal expansion and Young's modulus of MOX fuels [20].
- The coupling with the SCIANTIX module for the mechanistic modelling of inert gas behaviour [15,21].

The extension of the MACROS code concerned only the implementation of the novel correlations for the thermal expansion and Young's modulus of MOX fuels [20].

The present paper focuses on the assessment of the versions of GERMINAL, MACROS and TRANSURANUS extended in INSPYRE, called "post-INSPYRE".[1] This assessment aims at evaluating the impact of the novel models developed and implemented during the Project on the predicted fuel pin performance, validating the code extensions for application to fast reactor and Generation IV case studies.

The post-INSPYRE code versions are used to simulate two pins irradiated in the Phénix sodium-cooled fast reactor during the SUPERFACT-1 experiment: the SF13 fuel pin bearing 2 wt.% of ^{237}Np and the SF16 pin bearing 1.8 wt.% of ^{241}Am, both pertaining to the homogeneous minor actinide transmutation strategy. They reached a peak fuel burn-up at the end of irradiation of about 6.4 at.% (radial average value) [22]. The reader is referred to [14] for complete details about the SUPERFACT-1 irradiation experiment (i.e., description of the campaign, specifications of the pins, irradiation history and boundary conditions). The simulation options are the same as in [14], apart from the use of the new models developed and implemented during INSPYRE.

The simulation results from the post-INSPYRE FPCs concerning the fuel pins selected are herein presented and critically discussed, as well as compared with the pre-INSPYRE code results [14]. As in [14], the codes were validated against both integral and local post-irradiation examination data ([13,22,23]: cladding profilometry, fuel restructuring, radial profiles of Pu, Xe, Cs concentrations at the end of life) and benchmarked on the evolution of quantities of engineering interest, i.e., fuel central temperature, fuel restructuring, fuel-cladding radial gap size, and fission gas release.

The paper is organized as follows. Section 2 describes briefly the advanced models for properties of MOX fuels and mechanistic fission gas behaviour developed in the INSPYRE Project and adopted in the post-INSPYRE code simulations. The assessment and benchmark of the post-INSPYRE versions of the fuel performance codes GERMINAL, MACROS and TRANSURANUS is presented in Section 3. The comparison with the results of the reference (pre-INSPYRE) code versions [14] is included to highlight the differences in the pin performance results obtained. Section 4 identifies the main remaining gaps related to the simulation of MOX fuels in FR conditions and the key topics that should be the focus of future improvements. Conclusions are drawn in Section 5.

2. Overview of the modelling advancements for MOX fuels achieved in INSPYRE

The INSPYRE modelling efforts targeting fuel performance codes focused on the development and implementation of physics-based models and correlations for both thermal and mechanical properties of MOX fuels and for the description of fission gas and helium behaviour in oxide nuclear fuels [15].

Concerning the thermal properties, novel models for the thermal conductivity and melting (solidus) temperature of fast reactor-type MOX fuels were developed from the best fit of suitable and up-to-date experimental data, verified and validated against separate-effect measurements [16,17,24,25]. Comprehensive and physically-grounded laws depending on temperature, Pu and minor actinide (Am, Np) contents, deviation from fuel stoichiometry (corresponding to O/M = 2.00), porosity and burn-up were obtained and validated. The assessment included a p-value statistical analysis of the correlation coefficients (on the basis of the experimental dataset fitted), confirming the suitability and representativeness of the models proposed. Thanks to the fitting dataset selected, the correlations cover the values of interest for FR MOX and envisaged for Generation IV applications. In particular, the applicability ranges extend up to high temperatures (2700 K, close to fuel melting, for the thermal conductivity), as well as high Pu contents (50 at.%) and burn-up (12 at.%). These correlations were implemented in the GERMINAL and TRANSURANUS fuel performance codes [15] and used in this work to account for the effect of the Am and Np contents of SUPERFACT-1 on the fuel thermal properties.

For the sake of completeness, although not employed for the post-INSPYRE simulations presented here, a novel law for the heat capacity of U–Pu oxide fuels was developed during INSPYRE, preliminarily implemented and tested in the GERMINAL and TRANSURANUS codes. It is applicable on the entire Pu content range (from UO_2 to PuO_2) and it represents the Bredig transition effect at high temperature (> 2000 K, depending on the MOX Pu content) through a heat capacity peak, on the basis of atomic scale calculations [18,19].

As for the mechanical properties, the modelling efforts of INSPYRE focused on the Young's modulus and thermal expansion of MOX fuels, which drives the decrease of the fuel-cladding gap size (determined by the relative fuel and cladding deformation dynamics), and hence is an essential parameter to evaluate the gap conductance. The correlations developed, based on literature data for fast reactor-type MOX, cover a wide temperature range from room to melting temperature and include the effects of Pu content, fuel stoichiometry, porosity and burn-up (concentrations of fission products) [20]. These correlations were implemented in the post-INSPYRE versions of the three FPCs involved in INSPYRE [15].

In addition, the extension of the GERMINAL and TRANSURANUS FPCs included the development of SCIANTIX [15,21] and its coupling with the codes as a module. SCIANTIX is a grain-scale code developed at Politecnico di Milano that models the behaviour of inert gases (fission gases Xe, Kr, as well as helium) by using a cluster dynamics (rate theory) approach [26], and solves the physics-based master equations via fast and stable numerical techniques [27,28]. The current SCIANTIX modelling enables the treatment of both the intra-granular and inter-granular behaviour of inert gases. It also includes a fuel burn-up module targeting the helium production

[1] CEA performed the work presented here using GERMINAL V2.2.5, SCK CEN using the MACROS code, while ENEA, JRC-Karlsruhe and Politecnico di Milano employed version v1m5j20 of the TRANSURANUS code, including the new models developed in INSPYRE.

and allowing the tracking of the fuel composition evolution in terms of the most relevant actinides [29]. Finally, it describes the formation and gas depletion of the High Burn-up Structure (HBS) at the fuel pellet periphery [30]. The intra-granular part of the overall model considers single-gas atom diffusion, the three fundamental mechanisms of gas bubble nucleation, re-solution of gas atoms from bubbles and trapping of gas atoms at bubbles, and accounts for the coarsening of intra-granular bubbles along dislocation lines via vacancy inflow [31]. The inter-granular bubble evolution model currently available in SCIANTIX is the one proposed by Pastore et al. [32,33], which includes bubble interconnection allowing the fission gas release in the fuel-cladding gap. It was extended to consider the micro-cracking of grain boundaries during temperature transients, which induce burst releases of the fission gas stored at the grain boundaries [34,35]. Both the intra- and inter-granular components of fuel gaseous swelling result from this mechanistic description of fission gas behaviour, being connected to the evolution of the bubble populations and calculated according to the bubble concentration and radius [21]. The modelling of helium behaviour relies on the model by Cognini et al. [36] accounting for helium diffusivity and solubility [37,38]. It was extended to couple the inter-granular helium treatment to the intra-granular one [39]. Finally, the HBS modelling was recently improved with the inclusion of the inter-granular porosity evolution under irradiation in oxide fuels [40].

SCIANTIX was coupled with the GERMINAL and TRANSURANUS fuel performance codes as an inert gas behaviour module. It is called by the FPCs at each point of the adopted fuel radial mesh, in each axial slice discretizing the fuel column. The coupling strategy between the two codes and SCIANTIX, however, differs in some aspects, i.e., some of the SCIANTIX models were adjusted in GERMINAL by introducing limiting maximum thresholds (e.g., on the fuel grain growth and on the grain-boundary gas concentration upon saturation) [15,41]. The online coupling between TRANSURANUS and SCIANTIX has been achieved by means of a dedicated Fortran95/C++ interface, based on modern Fortran features as interface modules [15,42,43].

The novel, common models (among those described in this Section) implemented in the FPCs and employed in the present work for the simulation (post-INSPYRE) of the SUPERFACT-1 irradiation experiment are summarized in Table 1.

3. Assessment against experimental data and benchmark of INSPYRE-extended codes

This Section presents the assessment of the post-INSPYRE code versions on the available experimental data and the benchmark between the three codes on relevant quantities not measured during the SUPERFACT-1 experimental campaign, in line with the analysis performed in [14] using the pre-INSPYRE code versions. The comparison between pre- and post-INSPYRE code results is given for all the results presented below (left and right plots, respectively), to highlight and analyse the differences in the pin performance determined by the novel INSPYRE models implemented in the fuel performance codes.

3.1. Validation against integral and local experimental data

The most relevant integral code results on the Am-bearing pin SF16 [13,14] are collected and compared to the experimental data in Table 2. The values predicted by the pre-INSPYRE code versions, presented in [14], are also reported in round brackets. The agreement of the code results with the end-of-life fuel burn-up measured and the amount of fission gas produced is satisfactory, although the burn-up reached at the peak power node is (more) underestimated by post-INSPYRE TRANSURANUS and MACROS, while still overestimated by GERMINAL. The predictions of final fuel burn-up are still within the associated experimental uncertainty, recalling that the experimental value is obtained from the neodymium radial concentration at the end of irradiation, measured by EPMA with an uncertainty of 8% [22,23]. The burn-up analysis performed by Walker et al. [22] reveals an increase of the local fuel burn-up at the end of irradiation, near the fuel central void formed by restructuring, attributed to Pu and Am radial redistributions. This local (maximum) burn-up corresponds to around 7.8 at.% and is reproduced by GERMINAL and TRANSURANUS, equipped with actinide redistribution models [7,44,45], with adequate accuracy (within the experimental uncertainty). The deviation between experimental and calculated end-of-life fuel burn-up could be determined by the uncertainty on the SUPERFACT-1 irradiation history, which however is not clearly indicated among the specifications of the experiment accessible by the authors.

The most noticeable improvement from the pre- to the post-INSPYRE simulation results concerns the fission gas release (FGR), reflecting the adoption of the SCIANTIX fission gas behaviour modelling in GERMINAL and TRANSURANUS. The fission gas production, also tracked by SCIANTIX, remains consistent between the two codes and accurate with respect to the value reconstructed from measurements of fission gas release and retention [13]. For both GERMINAL and TRANSURANUS, the fission gas release at the end of life predicted by post-INSPYRE codes is higher than the pre-INSPYRE one, leading to a remarkable agreement with the experimental measurement. This is the result of the physics-based modelling of the intra- and inter-granular fission gas behaviour provided to the FPCs by SCIANTIX [21], and also of the SCIANTIX model for burst releases of fission gases due to fuel micro-cracking during power transients [35,46]. The burst release model acts on the fission gas accumulated at the grain boundaries following release from the grains, and enhances the gas release in the fuel-cladding gap. This overcomes the direct (empirical) FGR driven by temperature and fuel burn-up employed e.g., by the standard version of TRANSURANUS for FR conditions. Further investigations of the FGR calculated by the post-INSPYRE FPCs is provided in Section 3.2 when analysing its evolution in time (Fig. 7). These results already show the suitability of the SCIANTIX models for fission gas production and behaviour adopted by the coupled TRANSURANUS//SCIANTIX and GERMINAL//SCIANTIX suites and applied to FR conditions.

The predicted axial length of central void formed in the fuel at the end of life (accounting for the highest and lowest axial locations where fuel restructuring is detected) is in line with the pre-INSPYRE one by using the post-INSPYRE version of GERMINAL, still underestimating the measurement. It is instead in line with the experimental value according to post-INSPYRE TRANSURANUS, whose result is lower compared to the pre-INSPYRE one consistently with a lower fuel temperature regime yielded by the calculations especially at beginning of irradiation (reported below, Fig. 5). The opposite effect is provided by MACROS calculations, since the fuel central void extension higher from the post-INSPYRE code and within the uncertainty range associated to the measured data. The reliability of the code results, however, is influenced by e.g., the axial fuel relocation, highly stochastic and not considered at present in TRANSURANUS, while completely allowed in GERMINAL [7,8,12].

Finally, the fuel column axial elongation at the end of life yielded by the post-INSPYRE versions of MACROS and TRANSURANUS is closer to the experimental value, but still overestimated. The axial elongation is on the contrary underestimated by GERMINAL. The axial relocation mechanism and the fuel-cladding gap closure and mechanical interaction, which are predicted in the early irradiation

Table 1
Summary of models for MOX fuels developed in the INSPYRE Project and implemented in the post-INSPYRE versions of the GERMINAL, MACROS and TRANSURANUS fuel performance codes [15], for their assessment against the SUPERFACT-1 irradiation experiment.

Property/Phenomenon	Model	References
Thermal conductivity	$k_0(T,x,[Pu],[Am],[Np],p) = \left(\frac{1}{A+BT}+\frac{D}{T^2}e^{-\frac{E}{T}}\right)(1-p)^{2.5}$ $k_{irr}(T,x,[Pu],[Am],[Np],p,bu) = k_{inf}+\left(k_0-k_{inf}\right)\bullet e^{-\frac{bu}{\phi}}$	[16,17,24,25]
Melting temperature	$T_{m,0}([Pu],x,[Am]) = T_{m,UO_2}-\gamma_{Pu}[Pu]-\gamma_x x-\gamma_{Am}[Am]$ $T_{m,irr}([Pu],x,[Am],bu) = T_{m,inf}+\left(T_{m,0}-T_{m,inf}\right)\bullet e^{-\frac{bu}{\delta}}$	[16,17,24,25]
Young's modulus	$E_0([Pu]) = E_{UO_2}(1-[Pu])+E_{PuO_2}[Pu]$ $E(p) = E_0\frac{(1-p)^2}{1+c_E\nu_0 p}$ $E(x) = E_0\left[1-x\left(\frac{1}{E_0}\frac{\partial E}{\partial x}\right)_{20\%\ Pu}\right]$ $E(T) = E_0\left[a_0+a_1\frac{T}{T_m}+a_2\left(\frac{T}{T_m}\right)^2\right]$	[20]
Thermal expansion	$\frac{\Delta L}{L_0}(T) = b_0+b_1\left(\frac{T}{T_m}\right)+b_2\left(\frac{T}{T_m}\right)^2+b_3\left(\frac{T}{T_m}\right)^3$ $\alpha_V = 3\frac{\frac{d}{dT}\left(\frac{\Delta L}{L_0}\right)}{1+\frac{\Delta L}{L_0}}\left[1+b_x\left(2-\frac{O}{M}\right)\right]$	[20]
Intra-granular fission gas behaviour	$\begin{cases}\frac{\partial}{\partial t}(c_1+m) = \frac{\alpha}{\alpha+\beta}D_c\frac{1}{r^2}\frac{\partial}{\partial r}r^2\frac{\partial}{\partial r}(c_1+m)+yF \\ \frac{d}{dt}N_{ig} = \nu-\alpha N_{ig}\end{cases}$ ig: intra-granular	[21,26,31]
Inter-granular fission gas behaviour	$\frac{\partial}{\partial t}q = -\left[\frac{3}{a}\frac{\alpha}{\alpha+\beta}D_c\frac{\partial}{\partial r}(c_1+m)\right]_{r=a}-R_{term}$	[21,32,33]
Inter-granular fission gas burst release	$\frac{df}{dt} = -\frac{dm_c(T)}{dT}\frac{dT}{dt}f$ $\frac{dF_c}{dt} = \frac{dF_c}{dt}_{diff}+\frac{df}{dt}F_c$	[21,34,35]
Fuel swelling	$\left(\frac{\Delta V}{V}\right) = \left(\frac{\Delta V}{V}\right)_{ig}+\left(\frac{\Delta V}{V}\right)_{gf} = \frac{4}{3}\pi N_{ig}R_{ig}^3+\frac{3}{a}\frac{4\pi}{3}N_{gf}R_{gf}^3$ ig: intra-granular, gf: grain-face	[21]

Symbols: α: bubble re-solution rate; α_V: volumetric thermal expansion coefficient (b_0, b_1, b_2, b_3, b_x: correlation coefficients); β: bubble trapping rate; ν: bubble nucleation rate; ν_0: Poisson's ratio; a: grain radius; [Am]: americium concentration; bu: burn-up; c_1: single-atom gas concentration; c_E: coefficient of the porosity-dependent Young's modulus model; D_c: single-atom diffusion coefficient; E: Young's modulus (a_0, a_1, a_2: coefficients of the temperature-dependent correlation); E_0: Young's modulus of fully-dense, stoichiometric MOX; F: fission rate; F_c: grain boundary fractional coverage (diff: contribution from diffusion-controlled processes); f: intact fraction of grain faces; k_0: fresh MOX thermal conductivity (A, B, D, E: correlation coefficients); k_{irr}: irradiated MOX thermal conductivity (k_{inf}, ϕ: correlation coefficients); $\frac{\Delta L}{L_0}$: relative linear deformation; m: gas concentration in intra-granular bubbles; $m_c(T)$: micro-cracking function; N: bubble concentration; [Np]: neptunium concentration; $\frac{O}{M}$: oxygen-to-metal ratio; p: porosity; [Pu]: plutonium concentration; q: inter-granular gas concentration; R: bubble radius; r: radial coordinate; R_{term}: inter-granular release term; T: temperature; t: time; T_m: melting temperature; $T_{m,0}$: fresh MOX melting temperature (γ_{Pu}, γ_x, γ_{Am}: correlation coefficients); $T_{m,irr}$: irradiated MOX melting temperature ($T_{m,inf}$, δ: correlation coefficients); $\frac{\Delta V}{V}$: fuel pellet relative volume variation; x: deviation from fuel stoichiometry; y: fission yield of fission gas.

cycles by the post-INSPYRE GERMINAL version for the peak power node, play a significant role in the estimated elongations of both fuel and cladding. Among the values calculated by the different codes, TRANSURANUS provides the highest fuel and cladding axial elongations at the end of irradiation, linked to the absence of fuel-cladding mechanical interaction, since gap closure is not predicted. MACROS also calculates a significant axial elongation of the fuel stack, allowed by a gap closure occurring at mid-irradiation (during the fourth irradiation cycle). The cladding axial elongation is quite well reproduced by TRANSURANUS, while it is underestimated by

Table 2
Comparison of experimental/reconstructed data [13,22] and simulation results of integral quantities regarding the americium-bearing fuel pin SF16, as calculated by post-INSPYRE codes. The values calculated by pre-INSPYRE codes are reported in round brackets [14].

	Data	Calculated TRANSURANUS	Calculated GERMINAL	Calculated MACROS
Final burn-up at peak power node, radial average (at.%)	6.4	6.32 (6.35)	6.60 (6.60)	6.34 (6.60)
Fission gas (Xe + Kr) produced (cm^3)	225.03	228.9 (226.4)	226.7 (226.7)	224 (236.4)
Fission gas release (%)	68.5	69.7 (47.0)	68.5 (53.2)	60.9 (53.8)
Central hole length (mm)	550–619	602.6 (691)	424.8 (424.7)	618.2 (541)
Fuel axial elongation (mm)	5.6–6.2	17.36 (25.50)	0.38 (0.47)	16.89 (39.13)
Cladding axial elongation (mm)	1.5–2.3	1.44 (1.43)	0.04 (−0.01)	0.73 (1.76)

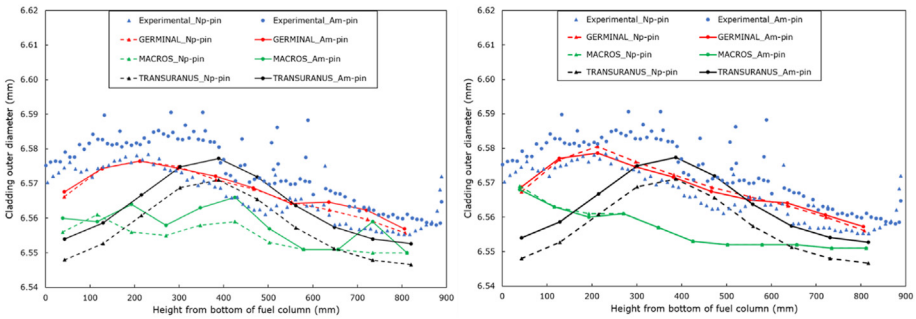

Fig. 1. Comparison of the cladding axial profilometry calculated at the end of life for the Np-bearing pin SF13 (triangles, dashed lines) and the Am-bearing pin SF16 (circles, full lines) with experimental measurements. The left plot reports the results from the pre-INSPYRE versions of the codes [14], while the right plot shows the post-INSPYRE code results.

both GERMINAL and MACROS. In general, the GERMINAL code yields the most stable results between the pre- and post-INSPYRE versions, as demonstrated by Table 2.

The cladding outer diameter results are shown in Fig. 1, along with the cladding profilometry data available from post-irradiation examinations. The cladding radial deformation at the end of life obtained using the post-INSPYRE code versions is similar to the pre-INSPYRE result for GERMINAL and TRANSURANUS. The post-INSPYRE TRANSURANUS results for the end-of-life cladding profilometry follow the axial profile of the linear pin power, for both Am- and Np-pins, as for the pre-INSPYRE code version. Accurate results are obtained around the peak power node, where the radial cladding deformation is the highest. TRANSURANUS yields the largest underestimations towards the ends of the fuel column, especially near the bottom of the stack. The post-INSPYRE GERMINAL calculations lead to slightly higher values than the pre-INSPYRE ones, yielding the best agreement with the experimental data for the Np-bearing pin but still underestimating slightly the measurements on the Am-bearing pin. The most significant difference between pre- and post-INSPYRE code results is shown by MACROS, whose post-INSPYRE version provides profiles almost superimposed for the Am- and Np-pins and more regular compared to the pre-INSPYRE ones. The post-INSPYRE MACROS version exhibits an acceptable agreement with the measured profilometry at the bottom and top of the pin, despite the general underestimation of the experimental profile. The post-INSPYRE code results on the end-of-life cladding profilometry confirm the outcomes of the pre-INSPYRE code assessment [14], i.e., that the different models of cladding creep and swelling in the codes have a noticeable impact on the simulation outcomes. This is enhanced by the fuel-cladding gap closure, which is predicted at the axial peak power node by GERMINAL and MACROS (for the Am-pin). The correct simulation of the cladding deformation is challenging since it is the result of the interplay between pellet-cladding interaction, radiation-induced (and potentially thermal) cladding creep and radiation-induced cladding swelling. The radiation-induced components dominate in the correlations applied in the codes and lead to an underestimation of the impact of the local temperature on the cladding profilometry. The remarkable agreement of the GERMINAL results with the data shows the importance of equipping the codes with a refined cladding swelling model based on a large experimental database, as that available in GERMINAL for 15-15Ti claddings [7,14]. Since the cladding modelling was not a focus of the INSPYRE Project, the discrepancies identified in the pre-INSPYRE code versions [14] remain in the post-INSPYRE versions.

The comparison of the pre- and post-INSPYRE versions of the MACROS code allows identifying the separate impact of the novel models for the fuel mechanical properties, i.e., the MOX Young's modulus and thermal expansion (since these are the only INSPYRE modelling advancements introduced in MACROS) [20]. In particular, the wider gap size evolving in time yielded by post-INSPYRE MACROS (from a lower fuel thermal expansion predicted) suggests a milder mechanical interaction between fuel and cladding, occurring just during the last irradiation cycle. This contributes to the lower radial deformation of the cladding at the end of life compared to the pre-INSPYRE result (Fig. 1). The effect of the fuel thermal expansion is not directly visible from GERMINAL and TRANSURANUS calculation results, since it is combined with the influence of the novel correlation for the MOX thermal conductivity [17] and of the novel modelling of fission gas release in the gap [15,21]. Anyway, the impact of the novel INSPYRE models (for the MOX fuel) on the predicted cladding profilometry proves to be limited since indirect, despite the different gap pressure calculated by the post-INSPYRE codes and the gap closure according to GERMINAL and MACROS (Section 3.2).

Figs. 2 and 3 show the code simulation results on fuel restructuring, i.e., concerning the formation and development of the fuel central void and of columnar grains, which are typical phenomena observed experimentally in MOX fuels irradiated in fast reactors at high temperature [47] and also in the SUPERFACT-1 fuels at the end of life. The trends yielded by the codes are all mainly determined by the axial pin power distribution, i.e., they exhibit peaks in both the fuel central void and the columnar grain size around the axial peak power node. Compared to the pre-INSPYRE results [14], the post-INSPYRE code results correspond to generally lower fuel restructuring, consistently with the lower fuel central temperature regimes at beginning of irradiation (see Fig. 5), in particular in the TRANSURANUS case. This leads to an underestimation of the experimental fuel central void by TRANSURANUS, while the pre-INSPYRE results were in excellent agreement with the measurements available, as shown in Fig. 2. The post-INSPYRE GERMINAL and MACROS versions still overestimate the data on the fuel central void size around the axial peak power node, but are more accurate at the upper part of the fuel column. The experimental values at the top of the fuel column (i.e., absence of fuel restructuring) are correctly caught by all the post-INSPYRE code versions, as a consequence of fuel central temperature regimes below the threshold for fuel inner void formation (1800°C, based on experimental data [9,48]). This also determines a locally lower extent of fuel restructuring predicted by post-INSPYRE TRANSURANUS and the absence of central void re-opening in the Np-pin from post-INSPYRE GERMINAL (Fig. 2 – right). The post-INSPYRE version of the MACROS code still provides the highest fuel central void radius at mid-column (~1.2 mm for the Am-pin, ~1.3 mm for the Np-pin), which is not the case for the extension of the columnar grains, as shown by Fig. 3. The radial extension of columnar grains calculated by post-INSPYRE MACROS is also similar to the pre-INSPYRE ones (due to the fact that only the novel models for mechanical

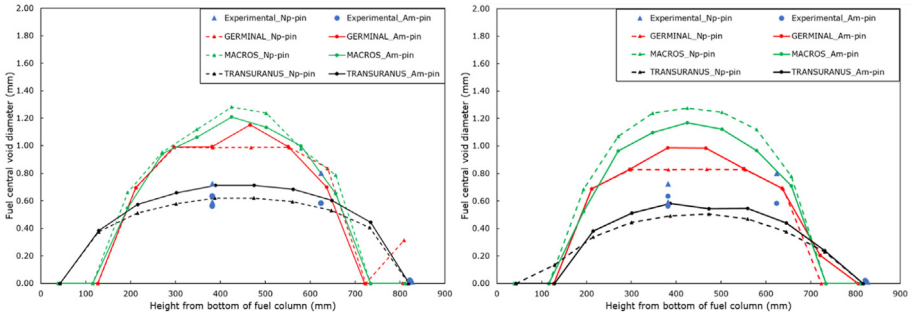

Fig. 2. Comparison of the axial profile of fuel central void diameter calculated at the end of life for the Np-bearing pin SF13 (triangles, dashed lines) and the Am-bearing pin SF16 (circles, full lines) with experimental measurements. The left plot reports the results from the pre-INSPYRE versions of the codes [14], while the right plot shows the post-INSPYRE code results.

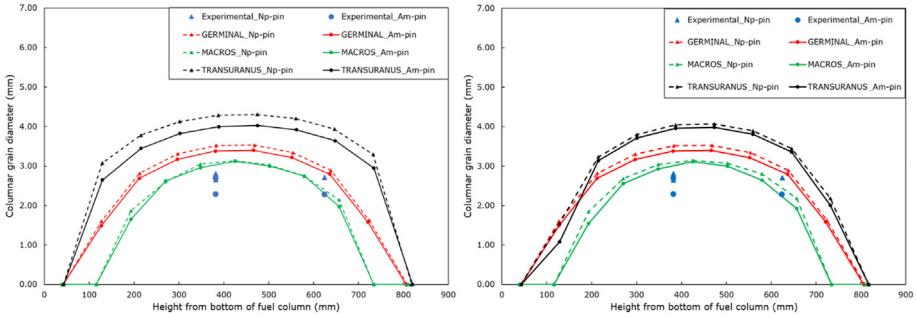

Fig. 3. Comparison of the axial profile of columnar grain diameter calculated at the end of life for the Np-bearing pin SF13 (triangles, dashed lines) and the Am-bearing pin SF16 (circles, full lines) with experimental measurements. The left plot reports the results from the pre-INSPYRE versions of the codes [14], while the right plot shows the post-INSPYRE code results.

properties have been adopted in MACROS, Section 2) and still the most accurate with respect to the experimental data. The post-INSPYRE models, however, allow for a homogenization of the code results. In particular, the post-INSPYRE TRANSURANUS predictions are closer to the ones from GERMINAL and MACROS, again due to the lower temperature regime at beginning of irradiation (Fig. 5), and hence closer to the measurements available, despite the global overestimation (Fig. 3 – right). The axial profile of columnar grains from post-INSPYRE TRANSURANUS is less extended, consistently with the axial shape of the fuel central void (Fig. 2). Hence, among the novel models developed during the INSPYRE Project (Section 2), the fuel restructuring results, which are mainly driven by the fuel temperature regime, are affected mostly by the fuel thermal conductivity and by the fuel thermal expansion and fission gas release, which contribute to the gap size and composition evolution, respectively. The similar pre- and post-INSPYRE GERMINAL results on fuel restructuring are caused by the similar evolutions of the fuel central temperatures. On the contrary, the pre- and post-INSPYRE MACROS versions yield similar results for the Am-pin despite the sensibly lower fuel central temperature during irradiation emerging from the post-INSPYRE code (shown in Fig. 5 – right for the peak power node).

The comparison of the post-INSPYRE code results with the experimental radial profile of plutonium concentration at the end of life is reported in Fig. 4 – right. Compared to the pre-INSPYRE results ([14], Fig. 4 – left), the post-INSPYRE profiles are generally similar for each code and GERMINAL still provides the stronger Pu radial redistribution, corresponding to an overestimated Pu concentration at the central region of the pellets while underestimated at intermediate radii. Moreover, the post-INSPYRE GERMINAL

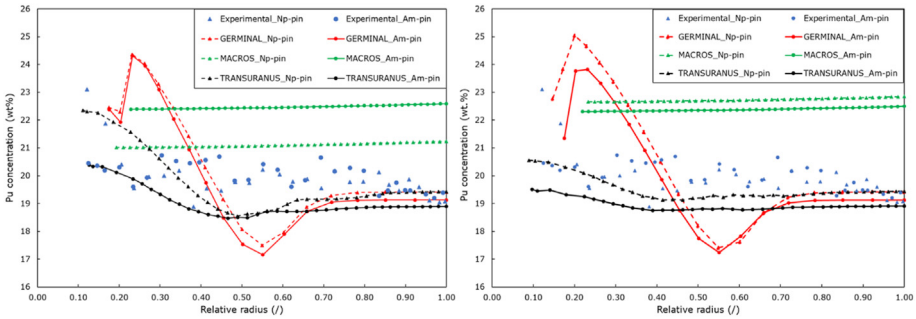

Fig. 4. Comparison of the plutonium radial concentration calculated at the end of life at the axial peak power node, for the Np-bearing pin SF13 (triangles, dashed lines) and the Am-bearing pin SF16 (circles, full lines), with experimental measurements. The left plot reports the results from the pre-INSPYRE versions of the codes [14], while the right plot shows the post-INSPYRE code results.

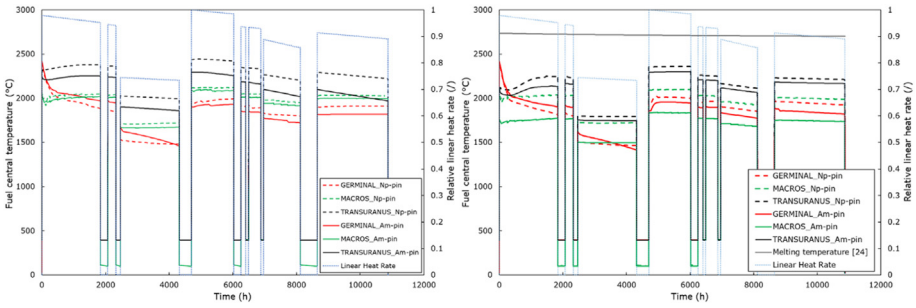

Fig. 5. Evolution of the fuel central temperature calculated along irradiation at the peak power node, for the Np-bearing pin SF13 (dashed lines) and the Am-bearing pin SF16 (full lines). The left plot reports the results from the pre-INSPYRE versions of the codes [14], while the right plot shows the post-INSPYRE code results.

profiles are still characterized by a concentration step in the proximity of the central void, caused by numerical reasons already reported in [14] (i.e., the different meshes used for the solution of the central void – finite volumes, and for the dynamics in the fuel material – finite elements). On the contrary, post-INSPYRE TRANSURANUS provides a smaller Pu redistribution, again mainly because of the lower fuel temperature regime at beginning of irradiation yielded by the post-INSPYRE code version (Fig. 5 – right). This leads to the underestimation of the Pu experimental data close to the fuel central void, while the agreement with the data in this pellet region was better by using pre-INSPYRE TRANSURANUS. The accuracy of both GERMINAL and TRANSURANUS is satisfactory at the colder pellet periphery. The post-INSPYRE MACROS results are radially flat as the pre-INSPYRE ones, since the modelling developments made in MACROS during INSPYRE did not involve the introduction of an actinide redistribution module. The significant overestimation of the radial Pu profiles at the end of life from post-INSPYRE MACROS is confirmed, as obtained from the pre-INSPYRE code version.

3.2. Code benchmark on the evolution of relevant quantities during irradiation

Fig. 5 shows the evolution during irradiation of the fuel central temperature at the axial peak power node. The dynamics obtained from post-INSPYRE code versions are consistent with those predicted by the pre-INSPYRE ones, but differences at the beginning and at the end of irradiation emerge. Also, higher temperature values towards the end of the SUPERFACT-1 irradiation are calculated particularly by post-INSPYRE TRANSURANUS, while lower values throughout the entire irradiation emerge from post-INSPYRE MACROS for the Am-bearing pin. The post-INSPYRE TRANSURANUS results show the dominant effect of the novel INSPYRE correlation for the fuel thermal conductivity (Section 2), implemented and adopted by both GERMINAL and TRANSURANUS for the outcomes presented in Fig. 5 – right. First, for fresh fuels or low burn-up conditions it is in line with the main open-literature correlation for FR oxide fuels (by Philipponneau [49], used as a standard in pre-INSPYRE GERMINAL). This produces a harmonization of the post-INSPYRE TRANSURANUS predictions at the beginning of irradiation (until the third irradiation cycle) compared to GERMINAL, whose results are slightly affected by the adoption of the novel correlation. Second, both post-INSPYRE GERMINAL and TRANSURANUS provide higher fuel central temperatures towards the end of irradiation, due to a stronger burn-up degradation of the thermal conductivity according to the novel model due to the exponentially decreasing formulation. The fuel temperature regime is also heavily impacted by the conductance of the fuel-cladding gap, determined by the gap size and FGR. The higher FGR provided by post-INSPYRE codes (Fig. 7 - right) contributes to the higher fuel temperatures during the final irradiation cycles of the SUPERFACT-1 experiment, especially according to TRANSURANUS. Nevertheless, the fuel still respects a margin to melting even from the TRANSURANUS simulations, as represented by the grey curve in Fig. 5 – right. The post-INSPYRE MACROS results show a much colder fuel in the Am-pin compared to the pre-INSPYRE result, which is not the case for the Np-pin whose fuel temperature is similar (slightly higher) to that yielded by the pre-INSPYRE code. The effect of the lower MOX thermal expansion (wider gap during irradiation) provided by the novel INSPYRE correlation [20], compared to the reference MACROS correlation [9], is hence coherent with the MACROS result for the fuel temperature of the Np-pin. Besides the effects of the novel models for fuel thermal conductivity, FGR and thermal expansion, the post-INSPYRE simulation results confirm some causes of discrepancy between the various codes already identified in [14], in particular the modelling of fuel relocation, fuel creep and swelling impacts on the gap size and conductance. The generally lower fuel central temperatures at the beginning of irradiation yielded by the post-INSPYRE code versions lead to the reduced fuel restructuring (Figs. 2 and 3) and plutonium radial redistribution (Fig. 4), already presented in Section 3.1.

The evolutions of the fuel central void radius calculated at the peak power node are shown in Fig. 6. The post-INSPYRE TRANSURANUS result is slightly sensitive to the SUPERFACT-1 power variations, as the pre-INSPYRE one. The end-of-life values yielded by the post-INSPYRE TRANSURANUS version are lower than the pre-INSPYRE ones, consistently with the lower fuel central temperature regime at the beginning of irradiation (Fig. 5 – right) and with the axial profiles shown in Fig. 2 – right. On the contrary, the lower temperature along irradiation predicted by the post-INSPYRE MACROS version for the Am-pin does not impact the calculated central void size at the peak power node, while the central void in the Np-bearing pin results slightly larger than the corresponding pre-INSPYRE result. The evolution of fuel restructuring according to MACROS is still particularly impacted by the fourth start-up transient, leading to the highest power of the irradiation history, while the other SUPERFACT-1 power transients do not induce any effect on the fuel central void. Concerning the GERMINAL outcomes, the post-INSPYRE ones show a fast central void formation at the beginning of life, similarly to MACROS and TRANSURANUS but differently from the gradual increase of the fuel central void radius provided by the pre-INSPYRE calculations. Considering the same discrete finite element mesh employed in GERMINAL to represent the fuel pins [7,14] and the similar fuel temperature predictions at the beginning of life (Fig. 5), the different kinetics of central void formation (faster at beginning of irradiation) can be ascribed to the link between the modelling of pore migration towards the pellet

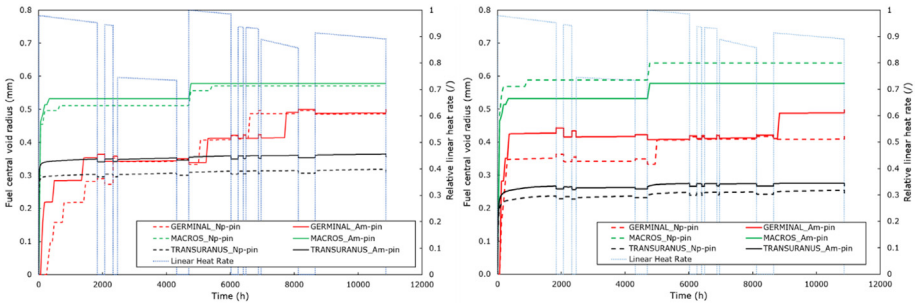

Fig. 6. Evolution of the fuel central void radius calculated along irradiation at the peak power node, for the Np-bearing pin SF13 (dashed lines) and the Am-bearing pin SF16 (full lines). The left plot reports the results from the pre-INSPYRE versions of the codes [14], while the right plot shows the post-INSPYRE code results.

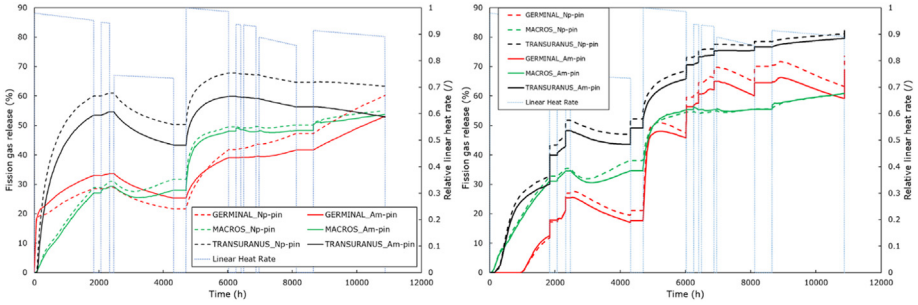

Fig. 7. Evolution of the fission gas release calculated along irradiation at the peak power node, for the Np-bearing pin SF13 (dashed lines) and the Am-bearing pin SF16 (full lines). The left plot reports the results from the pre-INSPYRE versions of the codes [14], while the right plot shows the post-INSPYRE code results.

centreline and the gaseous swelling that causes an increase of the porosity in fuel. This effect is determined by the novel inert gas models provided by the coupling of GERMINAL with SCIANTIX, which induces a lower fission gas release rate (hence, higher gas retention in the fuel) at the beginning of irradiation. Despite the different dynamics (more stable from post-INSPYRE GERMINAL after the first power rise), the end-of-life value is comparable to that of the pre-INSPYRE version for the Am-pin, while lower for the Np-pin.

The fission gas release calculated during the various irradiation cycles is shown in Fig. 7. The post-INSPYRE versions of the FPCs prove capable of reproducing end-of-life values of FGR during FR irradiations, in addition to the successful assessment against the integral FGR value measured on the SUPERFACT-1 pins (Table 2). These values correspond to an enhancement of the pre-INSPYRE predictions, which were in the range 50–60%, as shown by Fig. 7 – left. Also, the dynamics of FGR evolution during the SUPERFACT-1 irradiation cycles are different between pre- and post-INSPYRE codes, particularly concerning GERMINAL and TRANSURANUS, whose pre-INSPYRE FGR results mostly follow the power variations. Compared to the pre-INSPYRE result, the FGR evolution calculated by post-INSPYRE GERMINAL presents an initial incubation time for fission gas (longer than that shown by post-INSPYRE TRANSURANUS), and the release then occurs in bursts (i.e., sudden FGR bumps) associated to the micro-cracking of the grain boundaries [34,35], which occurs during power (temperature) transients and mostly during the power shutdowns. This is common also to post-INSPYRE TRANSURANUS and the same behaviour was obtained from the simulation of the sodium-cooled ASTRID case study, reported in [41]. Both the initial gas incubation time and the sudden gas releases during the SUPERFACT-1 inter-cycles are linked to the adoption of the SCIANTIX models for the treatment of fission gas behaviour. The incubation time reflects the processes of intra-granular diffusion of fission gases and their accumulation at the grain boundaries until saturation is reached [21,26]. The dynamics of burst releases of fission gas modelled by SCIANTIX and leveraged into fuel performance codes allows more aligned FGR evolutions between codes, despite still different values calculated during the irradiation cycles (determined by the many other aspects of the pin thermal-mechanical behaviour not covered in the present work, and modelled differently in different codes). This represents a remarkable proof of the importance and effectiveness of informing engineering-level FPCs with a physics-based modelling of lower-length scale processes, as achieved during INSPYRE via the coupling of FPCs with the SCIANTIX module for fission gas behaviour. The evolution according to post-INSPYRE MACROS resembles the pre-INSPYRE one, which could be expected since MACROS was not coupled with the SCIANTIX models.

The FGR in the fuel-cladding gap has a thermal feedback (via the gap conductance) on the fuel temperature regime predicted by post-INSPYRE codes (Fig. 5), especially GERMINAL and TRANSURANUS which benefited from the coupling with SCIANTIX. The gap conductance is also determined by the residual width of the fuel-cladding gap. GERMINAL predicts a fast gap closure during the first irradiation cycle and a gap continuously closed until the end of irradiation for both the Am- and Np-bearing pins, in line with the pre-INSPYRE result presented in [14]. Instead, the post-INSPYRE TRANSURANUS version yields a higher residual gap size at the peak power node for both the Am- and Np-pins compared to the pre-INSPYRE result [14], due to the enhanced FGR caused by the fuel micro-cracking which corresponds to a lower fuel gaseous swelling (i.e., determined by fission gas accumulation in intra- and inter-granular bubbles). Hence, the post-INSPYRE TRANSURANUS version still provides the slowest gap size reduction, leading to the hottest fuel along irradiation. The correct estimation of the gap residual width remains particularly challenging for fuel performance codes, since determined by the differential thermal expansion and radial deformations of fuel and cladding, induced also by

fuel fragmentation and relocation, creep and swelling processes (both depending on temperature and irradiation).

4. Remaining modelling gaps and further developments

The assessment of the capabilities of the GERMINAL, MACROS and TRANSURANUS code versions developed during the INSPYRE Project on two fuel pins (SF13 and SF16) from the SUPERFACT-1 irradiation experiment demonstrates some advancements in the simulation of the MOX fuel behaviour under FR conditions. In particular, the novel, mechanistic models for the fission gas behaviour in oxide fuels, provided to the fuel performance codes via the coupling with SCIANTIX [15,21], allow reproducing typical end-of-irradiation values of FGR in FR pins and harmonizing the predictions from different FPCs (Fig. 7). The consideration of the burst release contributions to the FGR, caused by the micro-cracking during power transients of FR fuels, proves to be important in this respect. Additionally, the novel correlations for the thermal-mechanical properties of MOX, particularly the thermal conductivity and thermal expansion, show a relevant impact on the fuel temperature results (Fig. 5) and related fuel restructuring (Figs. 2, 3 and 6), which are more consistent between codes at least at the beginning of irradiation, before substantial burn-up effects emerge. Despite this, the benchmark of the post-INSPYRE codes clearly evidences significant discrepancies in the evolution of the pin thermal behaviour. The integral validation of the post-INSPYRE versions of the three fuel performance codes exhibits a promising agreement with the available experimental data [13,22,23]. The radial concentration profiles in the fuel obtained at the end of life for actinides (Pu, as shown by Fig. 4), fission gases and fission products (presented for the pre-INSPYRE codes in [14]), however, still exhibit accuracy gaps. Hence, the comparison of the pin performance results obtained from the post-INSPYRE code versions with both the pre-INSPYRE ones [14] and the experimental data allows the identification of various improvement paths.

First, the current GERMINAL//SCIANTIX and TRANSURANUS//SCIANTIX coupled suites [15] are open to further adaptations and developments tackling FR irradiation conditions. Among the improvements needed, a proper modelling of the normal growth of FR fuel grains seems dominant, currently limited in GERMINAL while switched off in TRANSURANUS for FR irradiation conditions [15,41] (since the model currently available in the code is tailored for thermal - light water - conditions [50]). The fuel grain growth impacts the diffusion of fission gases across the pellet radius and the fuel gaseous swelling, by acting on the intra- and inter-granular gas concentrations. In this respect, the analysis of the radial concentration profiles of fission gases retained in the pellet, by comparing the code predictions and the available experimental data, reveals room for further improvements. The higher gas retention predicted by the codes in the inner part of the fuel pellet suggests further investigations on the equilibrium between the gas trapping and re-solution mechanisms inside the grains. Moreover, the inaccurate (lower) Xe retention predictions in the outer fuel region (i.e., at the colder pellet periphery) also indicates the need of assessing the athermal contribution to the fission gas diffusion coefficient [51]. The behaviour of fission gases at the pellet periphery could also be improved by means of a physics-based model for the high burn-up structure formation in the cold rim of oxide fuels, recently published in [40]. The integration in FPCs of the mechanistic framework offered by SCIANTIX paves the way for the inclusion of more and more physics-based models of fuel properties and phenomena.

The feedback of fuel restructuring on the intra-granular diffusion shall also be investigated, since the formation of columnar grains in the central part of the pellet does not affect in the same way the diffusion of the gases towards the grain boundaries, as in the fuel region under isotropic grain growth. Other modelling advancements that should provide an additional contribution to the physics-based fission gas release predicted by the SCIANTIX module is the consideration in the fuel performance code framework of the grain boundary venting [52] and of the role of open fabrication porosity (on the basis of e.g., [53]). Efforts along these directions are ongoing for the TRANSURANUS code, to obtain a TRANSURANUS//SCIANTIX coupled suite covering a wide set of physical aspects affecting the behaviour of mixed U–Pu oxide fuels under FR irradiation conditions.

For what concerns the radial concentration profiles of actinides at the end of life (e.g., Pu, Fig. 4), the results obtained from post-INSPYRE codes highlight the need to acquire more reliable mobility data for the GERMINAL and TRANSURANUS codes, and the implementation of a redistribution module for the MACROS code. Recent results on plutonium self-diffusion have been obtained in the framework of INSPYRE and presented in [54,55], and the consideration of these data for future versions of the GERMINAL and TRANSURANUS codes is planned.

Other code improvements recognized from the present work concern the modelling of the fuel-cladding gap dynamics, which impacts significantly (together with the fuel thermal conductivity) the fuel temperature profile and its evolution during irradiation. Modelling discrepancies concern the way different codes (GERMINAL and TRANSURANUS especially) treat fuel radial relocation, both regarding the fuel displacement before gap closure and the relocation accommodation after gap closure. GERMINAL accounts for a complete accommodation of cracks opened by fuel relocation after the gap closure [7], which is in line with a model implemented in the recent FUTURE code targeting the design of an ADS in China [56], while TRANSURANUS currently does not allow any relocation recovery, neither in the axial nor in the radial direction. Developments are ongoing to include in TRANSURANUS the modelling of a partial recovery of fuel fragments based on an empirical modelling approach [57]. Then, as pointed out by the strongly different gap evolutions (and consequently, different gap heat transfer), the modelling of gap conductance in the codes, currently accounting in different ways for gap closure and fuel-cladding mechanical interaction [7,58], would benefit from additional accurate separate-effect measurements, especially for beginning-of-life conditions. A deeper analysis of the various gap conductance models currently applied could also contribute to further reduce the spread in the predicted fuel central temperatures at the beginning of irradiation (Fig. 5). In addition, at high fuel burn-up, the code comparison pointed out the need to implement a model accounting for the JOG (Joint Oxide-Gaine) [59–61] formation and evolution in TRANSURANUS and MACROS, which is instead already modelled in GERMINAL [7].

Finally, the substantial differences that remain between the code results (in terms of both values and dynamics) concerning the gap evolution under irradiation also call – besides fuel relocation – for a more accurate description of the cladding, considering both temperature- and irradiation-driven phenomena e.g., cladding creep and swelling. The current and different cladding modelling in fuel performance codes leads to significant discrepancies in the predicted cladding profilometry, as shown by Fig. 1. In particular, the code calculations lack accuracy with respect to the available data at the colder pin extremities, pointing to a revision and improvement of the current modelling of irradiation-induced cladding deformations, which predominate at that pin locations. The consideration of the 15-15Ti cladding behaviour in FR and Generation IV conditions (i.e., high fast neutron fluxes and high temperature gradients) is out of the scope of the INSPYRE Project, which focuses on the MOX fuel itself, but it is the subject of the ongoing H2020 European Projects GEMMA [62] and Il Trovatore

[63]. The set of improvements needed in FPCs on the cladding side would benefit from the exchange of information between European Projects.

5. Summary and conclusions

We have presented in this paper an integral assessment and benchmark of the latest versions of the GERMINAL, MACROS and TRANSURANUS fuel performance codes, equipped with models developed in the INSPYRE H2020 European Project, addressing the thermal-mechanical properties and fission gas-related phenomena of MOX fuels under irradiation in FR conditions. This work is the second step after the first assessment [14] of the codes' capabilities prior to the INSPYRE developments ("pre-INSPYRE"). The modelling advancements implemented in the "post-INSPYRE" code versions concern the MOX thermal conductivity and melting temperature, thermal expansion and Young's modulus, and the physics-based treatment of fission gas behaviour (intra- and intergranular dynamics) and release, by means of the coupling of FPCs with the SCIANTIX meso-scale tool.

The extended versions of the three codes are herein applied again to two pins irradiated during the SUPERFACT-1 experiment. These pins feature a homogeneous minor actinide-bearing MOX fuel (doped with ~2 wt.% of Am and Np) and were irradiated up to an intermediate fuel burn-up. The integral code validation is performed against the available experimental data from post-irradiation examinations, and the comparison between the pre-INSPYRE and post-INSPYRE versions of each code is also presented, in order to evaluate the impact of the novel models on the integral pin performance and to highlight further development needs.

The code validation against local and integral experimental data reveals harmonized predictions of fuel temperature at the beginning of irradiation and hence of fuel restructuring (i.e., formation of a fuel inner void and columnar grains), but still significant differences on the end-of-life cladding profilometry (especially at the colder fuel column extremities) and on the radial profile of Pu redistribution. Also, the evolution in time of the fuel temperature predicted by the different codes is sensibly different at extended burn-up when relevant irradiation effects emerge. The spread among the results of different FPCs is fundamental to be considered for future code applications to design studies targeting advanced fuel pins for Generation IV reactors.

A substantial step forward is achieved for what concerns the predictions of fission gas release during FR irradiation, in terms of both kinetics and absolute values. The physics-based description of fission gas behaviour and release provided to the FPCs by the SCIANTIX module (coupled with GERMINAL and TRANSURANUS) allows the coherent consideration of various phenomena related to the behaviour of inert gases in oxide fuels, including the burst releases related to the fuel micro-cracking. The result is both a quantitative agreement with the reconstructed/experimental data on fission gas production and release and an alignment of the predictions from different FPCs. This achievement stresses the importance of including in fuel performance codes mechanistic models for as many material properties and pin phenomena as possible. SCIANTIX offers a multi-scale approach and environment designed to be easily extended and tailored by means of the model parameters or by considering additional gas-related mechanisms. Moreover, the combination of code developments and benchmarking performed in the INSPYRE Project has allowed identifying relevant gaps towards the reliable application of simulation tools to the fuel pin performance under FR irradiation conditions.

The SUPERFACT-1 pins considered are representative of Generation IV FR designs in terms of fuel composition (including minor actinides for transmutation purposes), cladding material (15-15Ti stainless steel) and irradiation conditions (i.e., temperature, linear power and neutron flux levels). The continuous assessment of the code simulation capabilities is key for their application to design and safety evaluations of fuel pins for future Generation IV, liquid metal-cooled reactor concepts. This is one main objective of fuel performance code developments and will be pursued during other European H2020 Projects, e.g., PuMMA [64], PATRICIA [65], currently in progress.

Declaration of competing interest

The authors declare that they have no known competing financial interests or personal relationships that could have appeared to influence the work reported in this paper.

Acknowledgments

This work has received funding from the Euratom research and training programme 2014–2018 through the INSPYRE project under grant agreement No 754329.

References

[1] GIF (Generation IV International Forum), GIF R&D Outlook for Generation IV Nuclear Energy Systems - 2018 Update", 2018.
[2] GIF (Generation IV International Forum), "Annual Report 2020", 2020.
[3] A.E. Waltar, D.R. Todd, P.V. Tsvetkov, Fast Spectrum Reactors, Springer, 2012.
[4] L. Luzzi, A. Cammi, V. Di Marcello, S. Lorenzi, D. Pizzocri, P. Van Uffelen, Application of the TRANSURANUS code for the fuel pin design process of the ALFRED reactor, Nucl. Eng. Des. 277 (2014) 173–187.
[5] A. Magni, T. Barani, F. Belloni, B. Boer, E. Guizzardi, D. Pizzocri, A. Schubert, P. Van Uffelen, L. Luzzi, Extension and application of the TRANSURANUS code to the normal operating conditions of the MYRRHA reactor", Nucl. Eng. Des. 386 (2022), 111581.
[6] EERA-JPNM, INSPYRE - Investigations Supporting MOX Fuel Licensing in ESNII Prototype Reactors", 2017 [Online]. Available: http://www.eera-jpnm.eu/inspyre/.
[7] M. Lainet, B. Michel, J.C. Dumas, M. Pelletier, I. Ramière, GERMINAL, a fuel performance code of the PLEIADES platform to simulate the in-pile behaviour of mixed oxide fuel pins for sodium-cooled fast reactors, J. Nucl. Mater. 516 (2019) 30–53.
[8] B. Michel, I. Ramière, I. Viallard, C. Introini, M. Lainet, N. Chauvin, V. Marelle, A. Boulore, T. Helfer, R. Masson, J. Sercombe, J.C. Dumas, L. Noirot, S. Bernaud, Two fuel performance codes of the PLEIADES platform: ALCYONE and GERMINAL, in: Nuclear Power Plant Design and Analysis Codes - Development, Validation and Application, Elsevier, 2021, pp. 207–233. Chap. 9.
[9] S.E. Lemehov, F. Jutier, Y. Parthoens, B. Vos, S. Van Den Berghe, M. Verwerft, N. Nakae, MACROS benchmark calculations and analysis of fission gas release in MOX with high content of plutonium, Prog. Nucl. Energy 57 (2012) 117–124.
[10] K. Lassmann, TRANSURANUS: a fuel rod analysis code ready for use, J. Nucl. Mater. 188 (C) (1992) 295–302.
[11] European Commission, TRANSURANUS Handbook, Joint Research Centre, Karlsruhe, Germany, 2020.
[12] A. Magni, A. Del Nevo, L. Luzzi, D. Rozzia, M. Adorni, A. Schubert, P. Van Uffelen, The TRANSURANUS fuel performance code, in: Nuclear Power Plant Design and Analysis Codes - Development, Validation and Application, Elsevier, 2021, pp. 161–205. Chap. 8.
[13] J.-F. Babelot, N. Chauvin, Joint CEA/JRC Synthesis Report of the Experiment SUPERFACT 1", 1999. Report JRC-ITU-TN-99/03.
[14] L. Luzzi, T. Barani, B. Boer, L. Cognini, A. Del Nevo, M. Lainet, S. Lemehov, A. Magni, V. Marelle, B. Michel, D. Pizzocri, A. Schubert, P. Van Uffelen, M. Bertolus, Assessment of three European fuel performance codes against the SUPERFACT-1 fast reactor irradiation experiment, Nucl. Eng. Technol. 53 (2021) 3367–3378.
[15] P. Van Uffelen, A. Schubert, L. Luzzi, T. Barani, A. Magni, D. Pizzocri, M. Lainet, V. Marelle, B. Michel, B. Boer, S. Lemehov, A. Del Nevo, Incorporation and verification of models and properties in fuel performance codes, INSPYRE Deliverable D7 2 (2020).
[16] A. Magni, L. Luzzi, P. Van Uffelen, D. Staicu, P. Console Camprini, P. Del Prete, A. Del Nevo, Report on the improved models of melting temperature and thermal conductivity for MOX fuels and JOG, INSPYRE Deliverable D6 2 (2020) version 2.
[17] A. Magni, T. Barani, A. Del Nevo, D. Pizzocri, D. Staicu, P. Van Uffelen, L. Luzzi, Modelling and assessment of thermal conductivity and melting behaviour of MOX fuel for fast reactor applications, J. Nucl. Mater. 541 (2020), 152410.

[18] E. Bourasseau, C. Takoukam-Takoundjou, D. Bathellier, Atomic scale calculation of heat capacity of MOX vs. composition, INSPYRE Deliverable D1 3 (2020).
[19] D. Bathellier, M. Lainet, M. Freyss, P. Olsson, E. Bourasseau, A new heat capacity law for UO_2, PuO_2 and $(U,Pu)O_2$ derived from molecular dynamics simulations and useable in fuel performance codes, J. Nucl. Mater. 549 (2021), 152877.
[20] S. Lemehov, New correlations of thermal expansion and Young's modulus based on existing literature and new data, INSPYRE Deliverable D6. 3 (2020).
[21] D. Pizzocri, T. Barani, L. Luzzi, SCIANTIX: a new open source multi-scale code for fission gas behaviour modelling designed for nuclear fuel performance codes, J. Nucl. Mater. 532 (2020), 152042.
[22] C.T. Walker, G. Nicolaou, Transmutation of neptunium and americium in a fast neutron flux: EPMA results and KORIGEN predictions for the SUPERFACT fuels, J. Nucl. Mater. 218 (2) (1995) 129–138.
[23] C. Prunier, F. Boussard, L. Koch, M. Coquerelle, Some specific aspects of homogeneous Am and Np based fuels transmutation through the outcomes of the SUPERFACT experiment in Phenix fast reactor, in: Proceedings of the Global '93 International Conference, vols. 12–17, 1993. September 1993, Seattle, USA.
[24] A. Magni, L. Luzzi, D. Pizzocri, A. Schubert, P. Van Uffelen, A. Del Nevo, Modelling of thermal conductivity and melting behaviour of minor actinide-MOX fuels and assessment against experimental and molecular dynamics data, J. Nucl. Mater. 557 (2021), 153312.
[25] A. Magni, P. Van Uffelen, A. Schubert, L. Luzzi, P. Del Prete, A. Del Nevo, Improved models of melting temperature and thermal conductivity for mixed oxide fuels doped with low minor actinide contents, INSPYRE Deliverable D6.5 (2022).
[26] D. Pizzocri, G. Pastore, T. Barani, A. Magni, L. Luzzi, P. Van Uffelen, S.A. Pitts, A. Alfonsi, J.D. Hales, A model describing intra-granular fission gas behaviour in oxide fuel for advanced engineering tools, J. Nucl. Mater. 502 (2018) 323–330.
[27] D. Pizzocri, C. Rabiti, L. Luzzi, T. Barani, P. Van Uffelen, G. Pastore, PolyPole-1: an accurate numerical algorithm for intra-granular fission gas release, J. Nucl. Mater. 478 (2016) 333–342.
[28] G. Pastore, D. Pizzocri, C. Rabiti, T. Barani, P. Van Uffelen, L. Luzzi, An effective numerical algorithm for intra-granular fission gas release during non-equilibrium trapping and resolution, J. Nucl. Mater. 509 (2018) 687–699.
[29] A. Cechet, S. Altieri, T. Barani, L. Cognini, S. Lorenzi, A. Magni, D. Pizzocri, L. Luzzi, A new burn-up module for application in fuel performance calculations targeting the helium production rate in $(U,Pu)O_2$ for fast reactors, Nucl. Eng. Technol. 53 (2021) 1893–1908.
[30] T. Barani, D. Pizzocri, F. Cappia, L. Luzzi, G. Pastore, P. Van Uffelen, Modeling high burnup structure in oxide fuels for application to fuel performance codes. Part I: high burnup structure formation, J. Nucl. Mater. 539 (2020), 152296.
[31] T. Barani, G. Pastore, A. Magni, D. Pizzocri, P. Van Uffelen, L. Luzzi, Modeling intra-granular fission gas bubble evolution and coarsening in uranium dioxide during in-pile transients, J. Nucl. Mater. 538 (2020), 152195.
[32] G. Pastore, L.P. Swiler, J.D. Hales, S.R. Novascone, D.M. Perez, B.W. Spencer, L. Luzzi, P. Van Uffelen, R.L. Williamson, Uncertainty and sensitivity analysis of fission gas behavior in engineering-scale fuel modeling, J. Nucl. Mater. 456 (2015) 398–408.
[33] G. Pastore, L. Luzzi, V. Di Marcello, P. Van Uffelen, Physics-based modelling of fission gas swelling and release in UO_2 applied to integral fuel rod analysis, Nucl. Eng. Des. 256 (2013) 75–86.
[34] G. Pastore, D. Pizzocri, J.D. Hales, S.R. Novascone, R.L. Williamson, B.W. Spencer, Modeling of transient fission gas behavior in oxide fuel and application to the BISON code, in: Proc. Enlarg. Halden Program. Group Meeting, 2014. Roros, Norway.
[35] T. Barani, E. Bruschi, D. Pizzocri, G. Pastore, P. Van Uffelen, R.L. Williamson, L. Luzzi, Analysis of transient fission gas behaviour in oxide fuel using BISON and TRANSURANUS, J. Nucl. Mater. 486 (2017) 96–110.
[36] L. Cognini, A. Cechet, T. Barani, D. Pizzocri, P. Van Uffelen, L. Luzzi, Towards a physics-based description of intra-granular helium behaviour in oxide fuel for application in fuel performance codes, Nucl. Eng. Technol. 53 (2) (2021) 562–571.
[37] L. Luzzi, L. Cognini, D. Pizzocri, T. Barani, G. Pastore, A. Schubert, T. Wiss, P. Van Uffelen, Helium diffusivity in oxide nuclear fuel: critical data analysis and new correlations, Nucl. Eng. Des. 330 (January) (2018) 265–271.
[38] L. Cognini, D. Pizzocri, T. Barani, P. Van Uffelen, A. Schubert, T. Wiss, L. Luzzi, Helium solubility in oxide nuclear fuel: derivation of new correlations for Henry's constant, Nucl. Eng. Des. 340 (2018) 240–244.
[39] R. Giorgi, A. Cechet, L. Cognini, A. Magni, D. Pizzocri, G. Zullo, A. Schubert, P. Van Uffelen, L. Luzzi, Physics-based modelling and validation of inter-granular helium behaviour in SCIANTIX, Nucl. Eng. Technol. 54 (2022) 2367–2375.
[40] T. Barani, D. Pizzocri, F. Cappia, G. Pastore, L. Luzzi, P. Van Uffelen, Modeling high burnup structure in oxide fuels for application to fuel performance codes. Part II: porosity evolution, J. Nucl. Mater. 563 (2022), 153627.
[41] A. Magni, D. Pizzocri, L. Luzzi, M. Lainet, B. Michel, Application of the SCIANTIX fission gas behaviour module to the integral pin performance in sodium fast reactor irradiation conditions, Nucl. Eng. Technol. 54 (2022) 2395–2407.
[42] D. Pizzocri, T. Barani, L. Luzzi, Coupling of TRANSURANUS with the SCIANTIX fission gas behaviour module, in: *International Workshop "Towards Nuclear Fuel Modelling in the Various Reactor Types across Europe"*, 18-19 June 2019, 2019. Karlsruhe, Germany.
[43] D. Pizzocri, L. Luzzi, T. Barani, A. Magni, G. Zullo, P. Van Uffelen, Coupling of SCIANTIX and TRANSURANUS: simulation of integral irradiation experiments focusing on fission gas behaviour in light water reactor conditions, in: International Workshop "Towards Nuclear Fuel Modelling In the Various Reactor Types across Europe, 2021, 28-30 June 2021, online.
[44] V. Di Marcello, A. Schubert, J. Van De Laar, P. Van Uffelen, Extension of the TRANSURANUS plutonium redistribution model for fast reactor performance analysis, Nucl. Eng. Des. 248 (2012) 149–155.
[45] V. Di Marcello, V. Rondinella, A. Schubert, J. Van De Laar, P. Van Uffelen, Modelling actinide redistribution in mixed oxide fuel for sodium fast reactors, Prog. Nucl. Energy 72 (2014) 83–90.
[46] D. Pizzocri, G. Pastore, T. Barani, E. Bruschi, L. Luzzi, P. Van Uffelen, Modelling of burst release in oxide fuel and application to the transuranus code, in: 11th International Conference on WWER Fuel Performance, Modelling and Experimental Support, vols. 15–21, 2019. September 2019, Varna, Bulgaria.
[47] F. Cappia, K. Tanaka, M. Kato, K. McClellan, J. Harp, Post-irradiation examinations of annular mixed oxide fuels with average burnup 4 and 5% FIMA, J. Nucl. Mater. 533 (2020), 152076.
[48] A. Gallais-During, F. Delage, S. Béjaoui, S. Lemehov, J. Somers, D. Freis, W. Maschek, S. Van Til, E. D'Agata, C. Sabathier, Outcomes of the PELGRIMM project on Am-bearing fuel in pelletized and spherepac forms, J. Nucl. Mater. 512 (2018) 214–226.
[49] Y. Philipponneau, Thermal conductivity of $(U, Pu)O_{2-x}$ mixed oxide fuel, J. Nucl. Mater. 188 (1992) 194–197.
[50] J.B. Ainscough, B.W. Oldfield, J.O. Ware, Isothermal grain growth kinetics in sintered UO_2 pellets, J. Nucl. Mater. 49 (2) (1973) 117–128.
[51] J. Turnbull, R. White, C. Wise, The diffusion coefficient for fission gas atoms in uranium dioxide, in: Technical Committee on Water Reactor Fuel Element Computer Modelling in Steady State, Transient and Accident Conditions, vols. 18–22, 1989. September 1988, Preston, United Kingdom.
[52] D. Pizzocri, T. Barani, L. Cognini, L. Luzzi, A. Magni, A. Schubert, P. Van Uffelen, T. Wiss, Synthesis of the inert gas behaviour models developed in INSPYRE, INSPYRE Deliverable D6. 4 (2020).
[53] A. Claisse, P. Van Uffelen, Towards the inclusion of open fabrication porosity in a fission gas release model, J. Nucl. Mater. 466 (2015) 351–356.
[54] P. Chakraborty, C. Guéneau, A. Chartier, Development of a complete thermo-kinetic description of cations in the mixed oxide of uranium and plutonium, in: *NuFuel-MMSNF 2019 Workshop*, 4-7 November 2019, PSI Villigen, Switzerland, 2019.
[55] P. Chakraborty, C. Guéneau, A. Chartier, Development of a thermokinetic model for Pu diffusion in $(U,Pu)O_{2\pm}$, INSPYRE Deliverable D5. 1 (2020).
[56] G. Wang, L. Gu, D. Yun, Preliminary multi-physics performance analysis and design evaluation of UO_2 fuel for LBE-cooled subcritical reactor of China initiative accelerator driven system, Front. Energy Res. 9 (October) (2021) 1–17.
[57] T. Preusser, K. Lassmann, Current status of the transient integral fuel element performance code URANUS, in: SMiRT, vol. 7, 1983, pp. 22–26. August 1983, Chicago, USA.
[58] M. Charles, M. Bruet, Gap conductance in a fuel rod: modelling of the FURET and CONTACT results, in: *Specialists' Meeting on Water Reactor Fuel Element Performance Computer Modelling*, 9-13 April 1984, Bowness-on-Windermere, United Kingdom, 1984.
[59] R.J. Parrish, F. Cappia, A. Aitkaliyeva, Comparison of the radial effects of burnup on fast reactor MOX fuel microstructure and solid fission products, J. Nucl. Mater. 531 (2020), 152003.
[60] F. Cappia, B.D. Miller, J.A. Aguiar, L. He, D.J. Murray, B.J. Frickey, J.D. Stanek, J.M. Harp, Electron microscopy characterization of fast reactor MOX Joint Oxyde-Gaine (JOG), J. Nucl. Mater. 531 (2020), 151964.
[61] M. Teague, B. Gorman, J. King, D. Porter, S. Hayes, Microstructural characterization of high burn-up mixed oxide fast reactor fuel, J. Nucl. Mater. 441 (1–3) (2013) 267–273.
[62] EERA-JPNM, GEMMA European H2020 Project", 2017 [Online]. Available: http://www.eera-jpnm.eu/gemma/.
[63] EERA-JPNM, Il Trovatore H2020 European Project, 2017 [Online]. Available: https://www.iltrovatore-h2020.eu/.
[64] European Union's Horizon 2020 Research and Innovation Programme, PuMMA H2020 European Project", 2020 [Online]. Available: https://pumma-h2020.eu/.
[65] European Union's Horizon 2020 Research and Innovation programme, PATRICIA - Partitioning and Transmuter Research Initiative in a Collaborative Innovation Action", 2020 [Online]. Available: https://patricia-h2020.eu/.